Stress Transfer From the Matrix to the Fibre in a Fragmentation Test: Raman Experiments and Analytical Modeling

ALKIS PAIPETIS AND COSTAS GALIOTIS
University of London
Queen Mary and Westfield College
Mile End Road
London E1 4NS, UK

YUNG CHING LIU AND JOHN A. NAIRN*
Material Science and Engineering
University of Utah
Salt Lake City, Utah 84112, USA

(Received July 8, 1997)
(Revised March 9, 1998)

ABSTRACT: The stress transfer properties of the fibre/matrix interface in the single fibre fragmentation test were investigated. Two carbon fibre-resin systems involving epoxy-sized and unsized fibres, were examined. Axial fibre stress data at resolutions of the order of one micron, were obtained with the technique of Remote Laser Raman Microscopy. Subsequent analytical modeling of the data was performed using a Bessel-Fourier Series stress analysis approach. The analysis provides a nearly exact solution for the stress field in the fragmentation test and simultaneously accounts for damaged or imperfect interfaces through the use of an interface parameter D_s. All data were fit using a two zone model in order to account for the propagation of interfacial damage as a function of applied strain. The fitting process was used to determine $D_s^{(i)}$, the interface parameter in undamaged zones, $D_s^{(d)}$, the interface parameter in the damage zones near fibre breaks, and l_d, the length of the damage zones, all as a function of applied strain. The interface parameter in the undamaged zones, $D_s^{(i)}$, was independent of applied strain. We claim $D_s^{(i)}$ is a good property for comparing fibre/matrix interfaces and the most relevant property for predicting the role to the interface in real laminates.

KEY WORDS: Raman Microscopy, Stress Transfer, Interface, Imperfect Interface

INTRODUCTION

IN THE SINGLE-FIBRE fragmentation test, a single fibre is embedded in a large amount of matrix and the specimen is loaded in tension. The tensile loading causes the fibre to break into fragments; the test is continued until the fragmentation process ceases [1]. The fragmentation process is influenced by the properties of the fibre/matrix interface; thus the single-fibre fragmentation test is widely used as a method for assessing interfacial properties. The question remains: how does one extract quantitative interfacial property information from the results of single-fibre fragmentation tests? Previous investigators have relied solely on fragment length *vs.* strain data or sometimes only on critical fragment length data which is the fragment length when the fragmentation process ceases. Such data is interpreted using simplistic elastic

---

[*] Author to whom correspondence should be addressed.

Author Prepared Reprint

plastic models [2], or elastic-plastic models in combination with simplistic, elastic, shear-lag models [3]. It is unlikely that such models can extract useful information from fragmentation data. By "useful," we mean quantitative interfacial properties that can be used to predict the role of the interface in real laminates. We claim it is additionally unlikely that *any* model could extract unambiguous information from fragmentation data alone. We need improved models and we need additional experimental observations on fragmentation specimens.

Here we have used Laser Raman Spectroscopy (LRS) during a fragmentation test as a tool to provide supplemental experimental observations about the fragmentation process. As has been demonstrated, LRS allows us to measure axial fibre stress in a composite with a spatial resolution of the order of 1 μm [4]. The fragmentation specimen provides an ideal configuration for LRS studies for both long [5, 6] and short reinforcing fibres [7]. Thus we can measure the axial fibre stress in fragments at any strain level during the fragmentation process. Previous LRS of embedded, single fibres has shown that the simplistic assumptions of elastic plastic models are inaccurate because the interfacial shear stress is not constant [5, 6]. LRS in regions of elastic stress transfer show that shear-lag models empirically predict fibre/matrix stress transfer [5, 6, 7]. Recent theoretical results, however, have shown that shear-lag analysis breaks down for low fibre volume fractions [8]. Thus, when shear-lag analysis is used to fit LRS results, the only information that results is an empirical determination of the shear-lag parameter. This parameter, however, cannot be related to interfacial properties for low fibre volume fraction specimens [8].

An improved stress analysis of the fragmentation test that can be useful in interpreting LRS results has been derived using a Bessel-Fourier series stress function in a full, axisymmetric stress analysis [9–11]. In brief, the Bessel-Fourier analysis is an exact elasticity solution (*i.e.*, the solution obeys equilibrium and compatibility). It further obeys all boundary conditions exactly except one. The single approximation is that the axial stress at the end of a broken fibre is equal to zero in an averaged sense instead of being uniformly equal to zero. Most elasticity analyses of fibre/matrix stress transfer assume a perfect interface. Such analyses are no help in interpreting fragmentation results because there is no interface property that can be varied to predict the role of the interface. In contrast, the Bessel-Fourier analysis in Ref. [9] accounts for an imperfect interface. The technique is to introduce an interface parameter, D_s, which is an effective stiffness for sliding of the fibre relative to the matrix under the influence of interfacial shear stress [12]. A value of $D_s = \infty$ corresponds to an perfect interface; a value of $D_s = 0$ corresponds to a debonded interface. Any other value of D_s represents an imperfect interface. We claim that using LRS to measure D_s during a fragmentation test is a potential method for characterizing the fibre/matrix interface [10]; the measured interfacial parameters have the potential to be used for studying the role of the interface in real laminates.

In this study, fragmentation tests with simultaneous LRS experiments were run on sized and unsized high modulus carbon fibres embedded in an epoxy resin. In a previous publication [4], the stress transfer characteristics of the two systems have been studied and different mechanisms of interfacial failure have been identified. In brief, a zone of damage appears near fibre breaks. Within the damage zone the rate of stress transfer is slower than when the interface is undamaged or in the central portion of fragments away from the damage zones. Clearly no single interface parameter, D_s, can predict the observed change in stress transfer properties between the damaged and undamaged zones. We thus modeled the experimental results using a two-zone, Bessel-Fourier analysis [9]. Within the damage zone $D_s = D_s^{(d)}$ where $D_s^{(d)}$ is the interface parameter for a damaged interface. We need not know precisely the mechanism of damage; we instead regard a measured value of $D_s^{(d)}$ as a measure of the ability of a damaged interface to transfer stress from the matrix to the fibre. Some physical effects that might play a role in the value of $D_s^{(d)}$ include interfacial cracks, interfacial friction, matrix yielding near the interface, and matrix cracks. In the undamaged, central portion of fragments $D_s = D_s^{(i)}$, where $D_s^{(i)}$ is the interface parameter for an undamaged or intact interface. We have measured $D_s^{(d)}$, $D_s^{(i)}$, and the size of the damage zone as a function of applied strain during a fragmentation test. $D_s^{(d)}$ decreases as strain increases indicating an increased impairment to stress transfer as interface damage becomes more extensive. In contrast, $D_s^{(i)}$ is independent of applied strain. We claim that $D_s^{(i)}$ is preferred over $D_s^{(d)}$ and over critical fragment length experiments as a measure of the fibre/matrix interfacial properties; it can be measured with LRS experiments.

MATERIALS AND METHODS

Laser Raman Spectroscopy (LRS) may be used to measure stresses in fibres in composites due to the stress or strain dependence of certain vibrational modes in the fibres [13]. Unique calibration curves are normally produced by stretching individual carbon fibres and recording the position of the carbon fibre peak as a function of either applied stress or strain. These calibration curves can afterwards be used to obtain stress or strain values of other similar fibres embedded in composites. LRS has been successfully used in applications involving a wide range of materials and specimen geometries, from single-fibre model composites [14] to real composite coupons [15]. LRS provides a unique tool for measuring internal stresses in composites.

Materials and Specimen Preparation

The sized and unsized high modulus fibres used in this study were provided by Soficar. The M40B-40B sized fibres are labeled MEBS; the M40B unsized fibres are labeled MUS. Both fibres have an effective diameter of 6.6 μm (as determined by density measurements) and a modulus of 390 GPa. The fibre strengths were determined at four gauge lengths for each fibre type. Both fibres were reported to have a standard level of oxidative treatment.

The fibres were embedded in an epoxy resin that was provided by Ciba-Geigy; it was a two part MY-750/HY-951 epoxy system. The resin (MY-750: unmodified liquid epoxy resin) and hardener (HY-951: triethylene tetramine) were mixed at 40°C at a ratio 4:1, degassed for 10 min under full vacuum and poured into silicon rubber dogbone moulds where individual fibres had previously been carefully aligned. The single-fibre composites were cured for 2 hrs at 60°C, removed from the moulds and subsequently post-cured at 120°C. The modulus, strength and approximate failure strain for the resin were 2.6 GPa, 65 MPa and 8%, respectively [4].

The cured dogbone samples were ground until the embedded fibre was approximately 100 μm away from the surface and then subsequently polished. A strain gauge was attached to the resin surface and the applied strain was derived from resistance measurements using a digital multimeter.

Specimen Testing and Raman Spectrum Acquisition

The LRS data acquisition was performed using the Remote Raman Microprobe (ReRaM). The ReRaM has been developed and tested in house, and uses flexible waveguides for both the delivery and the collection of light [4]. In addition, micrometer stages allow for the translation of the ReRaM in all three axes down to an accuracy of 1 μm. In this work, the laser was focused to a submicron spot on the specimen using a laser power of approximately 1 mW. The collected Raman light was guided through an optical fibre to a SPEX 1000M single monochromator. The Raman signal was collected via a Wright Instrument CCD and stored in a PC compatible computer. Spatial discrimination was achieved by magnification of the focal spot to fill the optical fibre end face.

Raman data were collected by scanning the Raman microprobe point-by-point along the embedded fibre. In general a section of the Fragmentation Gauge Length (FGL) of 2.5-3 mm in length, was scanned at different increments of externally applied load. Within this "window", measurements were taken at steps of 1 μm in the vicinity of fibre breaks where fibre stress is changing rapidly and then at steps of 2, 5 and 10 μm in regions away from fibre breaks where fibre stress changes more slowly.

The dogbone samples were mounted on a Hounsfield universal testing machine, and strained to strain levels of up to 5.00%. The strain rate was kept to a minimum (*i.e.*, 0.25×10^{-2} min^{-1}) in order to avoid relaxation effects. Fragmentation specimens with both sized and unsized specimens were tested until failure which occurred at approximately 8% strain.

Bessel-Fourier Analysis of Experiments

LRS experiments on fragmentation specimens can measure the axial stress in the fibre as a function of position along the fibre. To interpret these experiments, we fit the measured stress to a calculated stress based on a three-dimensional, axisymmetric stress analysis of stress transfer in fragmentation specimens in the presence of an imperfect interface [9]. The stress transfer analysis, which uses a Bessel-Fourier series stress function, accounts for an imperfect interface through an interface parameter, D_s. The fit to experimental results allows us to measure D_s and therefore to get a direct measure of the stress-transfer properties of the fibre/matrix interface.

The Bessel-Fourier series solution for the fragmentation specimen is described in detail in Ref. [9]; here we only quote those parts of the solution required to interpret LRS experiments. The average axial fibre stress in a fragment of length l is given by [9]:

$$\langle \sigma_{zz,f} \rangle = \psi_\infty \left(1 + \left\langle \sigma^{(p)}_{zz,f} \right\rangle \right) \tag{1}$$

where ψ_∞ is the axial stress in the fibre before there are any fibre breaks (the far-field fibre stress) and $\sigma^{(p)}_{zz,f}$ is the *perturbation* fibre stress. The far-field fibre stress is given by

$$\psi_\infty = \frac{\left(\frac{2\nu_A \nu_m}{E_A} - \frac{1-\nu_T}{E_T} - \frac{1+\nu_m}{E_m} \right) \frac{E_A \sigma_0}{E_m} + \left(\frac{2\nu_A}{E_A}(\alpha_T - \alpha_m) + \left(\frac{1-\nu_T}{E_T} + \frac{1+\nu_m}{E_m} \right)(\alpha_A - \alpha_m) \right) E_A \Delta T}{\frac{2\nu_A^2}{E_A} - \frac{1-\nu_T}{E_T} - \frac{1+\nu_m}{E_m}} \tag{2}$$

where E_A, E_T, ν_A, ν_T, α_A, and α_T are the axial and transverse tensile moduli, Poisson's ratios, and thermal expansion coefficients of the fibre. The fibre is assumed to be transversely isotropic with the axial direction along the axis of the fibre. The terms E_m, ν_m, and α_m are the modulus, Poisson's ratio, and thermal expansion coefficient of the assumed isotropic matrix. Finally, σ_0 is the applied axial stress during the fragmentation test and $\Delta T = T_s - T_0$ is the difference between the specimen temperature, T_s, and the stress-free temperature, T_0. The ΔT term accounts for residual stresses.

The solution in Eq. (1) is written as a superposition of the far-field stress with the perturbation stress. Physically, $\sigma^{(p)}_{zz,f}$ corresponds to the solution to the stress analysis problem of a single fibre fragment with a uniform compression stress of $\sigma_{zz} = -1$ applied to the ends of the fibre at $z = \pm l/2$ (note: the origin of the z axis is taken to be at the middle of the fibre fragment). Superposition of the far-field stress with the perturbation stress leads to solution in which the fibre stress is zero at fibre breaks. From Ref. [9], the *total* fibre axial stress is

$$\langle \sigma_{zz,f} \rangle = \psi_\infty \left(1 - \frac{F(z)}{F(l/2)} \right) \tag{3}$$

where the function $F(z)$ is defined by

$$\begin{aligned} F(z) &= \frac{E_A(1-\nu_T)}{2\left(\frac{1-\nu_T}{E_T} + \frac{1+\nu_m}{E_m} - \frac{2\nu_A^2}{E_A} \right)} \left[\frac{\nu_A a}{E_A} \left(\frac{1+\nu_m}{E_m} - \frac{1+\nu_T}{E_T} \right) - \frac{1}{G_T} \left(\frac{1-\nu_T}{E_T} + \frac{1+\nu_m}{E_m} \right) \right] \\ &\quad + \frac{d}{2} + 2 \sum_{i=1}^{\infty} \cos \frac{k_i z}{r_f} \left[c_{1i} \left(\frac{c}{s_1^2} - d \right) \frac{I_1(\beta_{1i})}{\beta_{1i}} + c_{2i} \left(\frac{c}{s_2^2} - d \right) \frac{I_1(\beta_{2i})}{\beta_{2i}} \right] \end{aligned} \tag{4}$$

and

$$\begin{aligned} a &= \frac{-\nu_A(1+\nu_T)}{1 - \frac{\nu_A^2 E_T}{E_A}} & c &= \frac{\frac{E_A}{G_A} - \nu_A(1+\nu_T)}{1 - \frac{\nu_A^2 E_T}{E_A}} \\ b &= \frac{\nu_T - \frac{\nu_A E_T}{E_A}\left(\frac{E_A}{G_A} - \nu_A \right)}{1 - \frac{\nu_A^2 E_T}{E_A}} & d &= \frac{\frac{E_A}{2G_T}(1-\nu_T)}{1 - \frac{\nu_A^2 E_T}{E_A}} \\ s_1^2 &= \frac{a + c + \sqrt{(a+c)^2 - 4d}}{2d} & s_2^2 &= \frac{a + c - \sqrt{(a+c)^2 - 4d}}{2d} \\ k_i &= \frac{2 r_f i \pi}{l} & \beta_{ji} &= \frac{k_i}{s_j} \end{aligned} \tag{5}$$

Here G_A and G_T are the axial and transverse shear moduli of the fibre and r_f is the radius of the fibre. The function $F(z)$ in Eq. (4) is written as a Bessel-Fourier series where $I_1(x)$ is the modified Bessel function of the first kind [17]. The terms c_{1i} and and c_{2i} are constants of the expansion that depend on fibre and matrix properties, on the fragment length, and on the fibre/matrix interface parameter (D_s). All c_{1i} and c_{2i} terms may be found by solving the following matrix equation for each term in the Bessel-Fourier series:

$$\begin{pmatrix} \left(a-\frac{1}{s_1^2}\right)\frac{I_1(\beta_{1i})}{s_1} & \left(a-\frac{1}{s_2^2}\right)\frac{I_1(\beta_{2i})}{s_2} & -K_1(k_i) & 2(1-\nu_m)K_1(k_i)-k_iK_0(k_i) \\ \left(a-\frac{1}{s_1^2}\right)I_0(\beta_{1i})+\frac{(1-b)}{s_1^2}\frac{I_1(\beta_{1i})}{\beta_{1i}} & \left(a-\frac{1}{s_2^2}\right)I_0(\beta_{2i})+\frac{(1-b)}{s_2^2}\frac{I_1(\beta_{2i})}{\beta_{2i}} & K_0(k_i)+\frac{K_1(k_i)}{k_i} & -(1-2\nu_m)K_0(k_i)+k_iK_1(k_i) \\ \frac{(b-1)}{s_1^2}\frac{I_1(\beta_{1i})}{2G_T\beta_{1i}} & \frac{(b-1)}{s_2^2}\frac{I_1(\beta_{2i})}{2G_T\beta_{2i}} & -\frac{K_1(k_i)}{2G_mk_i} & -\frac{K_0(k_i)}{2G_m} \\ \begin{gathered} -\left(\frac{1}{s_1^2G_A}-\frac{d+2\nu_Aa}{E_A}\right)I_0(\beta_{1i}) \\ -\left(\frac{1}{s_1^2}-a\right)\frac{\beta_{1i}I_1(\beta_{1i})}{D_s} \end{gathered} & \begin{gathered} -\left(\frac{1}{s_2^2G_A}-\frac{d+2\nu_Aa}{E_A}\right)I_0(\beta_{2i}) \\ -\left(\frac{1}{s_2^2}-a\right)\frac{\beta_{2i}I_1(\beta_{2i})}{D_s} \end{gathered} & \frac{K_0(k_i)}{2G_m} & \frac{1}{2G_m}\big(k_iK_1(k_i)-4(1-\nu_m)K_0(k_i)\big) \end{pmatrix} \begin{pmatrix} c_{1i} \\ c_{2i} \\ c_{3i} \\ c_{4i} \end{pmatrix} = \begin{pmatrix} 0 \\ (-1)^i\frac{4(1+\nu_T)}{k_i^2} \\ (-1)^i\frac{4(1-\nu_T)}{2G_Tk_i^2} \\ (-1)^i\frac{8\nu_A(1+\nu_T)}{E_Ak_i^2} \end{pmatrix} \tag{6}$$

where G_m is the shear modulus of the matrix, $K_0(x)$ and $K_1(x)$ are modified Bessel functions of the second kind [17], and D_s is the imperfect interface parameter. The extra constants found when solving Eq. (6) (c_{3i} and c_{4i}) are needed to determine the matrix stresses [9]. They are not needed here when finding only the axial stress in the fibre. This solution is for an anisotropic fibre embedded in an isotropic matrix. The solution *does not* include the solution for an isotropic fibre as a special case; the solution for an isotropic fibre is given in Ref. [9]. All results presented here are for anisotropic carbon fibres and therefore only the anisotropic-fibre result given above is needed. Finally, the solution is written as an *infinite* series. This series converges provided the number of terms is equal to or greater than the aspect ratio ($l/2r_f$) of the fibre fragment [9]. All analyses in this paper included sufficient terms to insure convergence.

Given fibre and matrix properties (see Table 1 for the properties used here for MEBS and MUS fibres and for the MY750 epoxy matrix), Eq. (1) determines the axial stress in the fibre except for the unknown interface parameter, D_s. The use of interface parameters in the analysis of composites was introduced by Hashin [12]. A definition of a perfect interface is that the radial and axial displacements are continuous from the fibre to the matrix. To include an imperfect interface, the displacements are allowed to be discontinuous. Hashin's imperfect interface model [12] assumes that the displacement discontinuities at the fibre/matrix interface are proportional to the associated interfacial stress; thus the radial, u, and axial, w, displacement discontinuities are given by

$$w_m(r_f)-w_f(r_f)=\frac{r_f\tau_{rz}(r_f)}{D_s} \qquad \text{and} \qquad u_m(r_f)-u_f(r_f)=\frac{r_f\sigma_{rr}(r_f)}{D_n} \tag{7}$$

where subscripts f and m denote fibre and matrix, $\tau_{rz}(r_f)$ and $\sigma_{rr}(r_f)$ are the interfacial shear and normal stresses, and D_s and D_n are interface parameters for displacement discontinuities in the axial and radial directions. Note that we have included a factor of r_f on the right hand side of the imperfect interface relations to give D_s and D_n units of stress; thus the units of D_s and D_n differ from the units used by Hashin [12]. As $D_s \to \infty$ and $D_n \to \infty$ the interface becomes a perfect interface (zero displacement discontinuities); as $D_s \to 0$ and $D_n \to 0$, the interface becomes debonded (zero interfacial stress); all other values for D_s or D_n are for an imperfect interface.

In Ref. [9], it was argued that the radial stresses in the fragmentation test are predominantly compressive. To prevent the matrix penetrating into the fibre (a negative radial displacement discontinuity), it is appropriate to set $D_n = \infty$. In other words, the role of the interface in fragmentation specimens can be modeled with a single interface parameter D_s. Mathematically, D_s corresponds to the magnitude of the axial displacement discontinuity at a two-dimensional interface. Physically it can correspond to any effect that influences fibre/matrix stress transfer. For example there may be an interphase of finite dimensions having different properties than the bulk matrix, there may be interfacial yielding, there may be debonding with friction, or there may be cracking into the matrix or fibre. Whatever interfacial mechanism influences stress transfer, we argue the results can be fit with an *effective* value for D_s that measures the ability of the interfacial zone or interphase to transfer stress from the matrix to the fibre. Furthermore, we argue that D_s is a useful interfacial property. It can, for example, be input into variational mechanics models to predict

Table 1. Thermal and mechanical properties used for the MEBS and MUS carbon fibres and for the MY750 epoxy matrix in the calculations in this paper.

Property	MEBS and MUS	MY750
Diameter ($2r_f$) (μm)	6.6	
Tensile Modulus (E_A or E_m) (GPa)	390	2.6
Transverse Modulus (E_T) (GPa)	14	
Axial Shear Modulus (G_A or G_m) (GPa)	20	0.97
Axial Poisson's Ratio (ν_A or ν_m)	0.20	0.34
Transverse Poisson's Ratio (ν_T)	0.25	
Axial CTE (α_A or α_m) (10^{-6}/°C)	-0.36	40
Transverse CTE (α_T) (10^{-6}/°C)	18	
Temperature Difference (ΔT) (°C)		-100

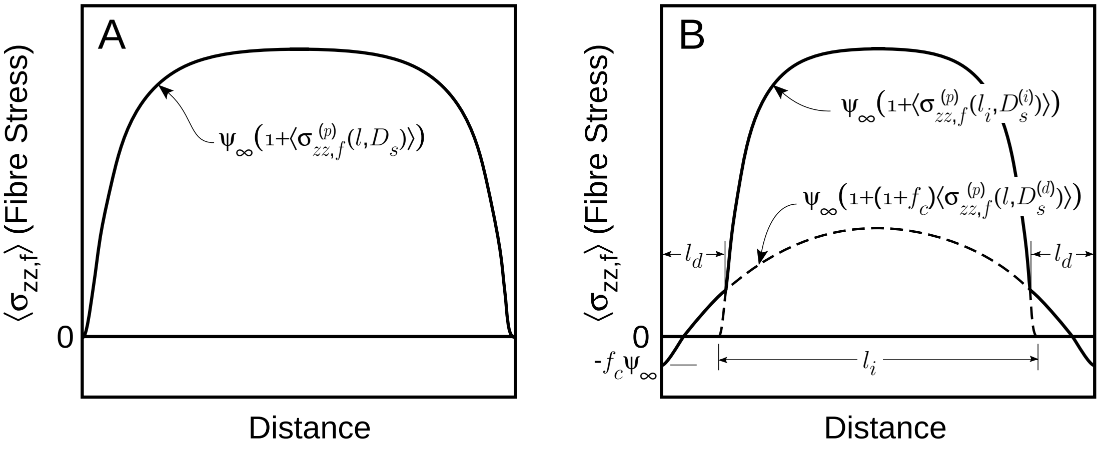

Figure 1. A. Typical calculation of the average axial stress in the fibre in a single fibre fragment from a fragmentation test using a constant value of the interface parameter, D_s. B. A modified analysis constructed to account for damage zones near fibre breaks and residual compressive stress on the ends of the fibre. $D_s = D_s^{(d)}$ in the damage zones near the fibre breaks and $D_s = D_s^{(i)}$ in the central, undamaged zone.

the effect of the interface on real laminates [12]. Thus an interface parameter measured in a single-fibre fragmentation test can be used to predict the properties of real laminates.

Figure 1A shows a typical calculation for axial fibre stress in a single fibre fragment from a fragmentation specimen when D_s is equal to a constant. Real experimental results show two effects that cannot be fit to such curves. First, fibre breaks in fragmentation specimens inevitably cause an interfacial damage zone near the fibre breaks. The stress transfer is different in the damage zone than in the undamaged, central region of the fibre fragment. No single value of D_s can fit a change in stress transfer rate within a single fragment; thus we fit experimental results using a two-zone model [9]. The two-zone model is illustrated in Fig. 1B. In brief, we assume $D_s = D_s^{(d)}$ in the damage zone and $D_s = D_s^{(i)}$ in the undamaged or intact zone. The two-zone analysis is constructed by analyzing a fragment of length l with $D_s = D_s^{(d)}$ and a fragment of length l_i with $D_s = D_s^{(i)}$. The value of l_i is selected such that the average fibre stress in the two zones are equal at the end of the observed damage zone of length l_d. Finally, the calculated stress comes from the $D_s = D_s^{(d)}$ results in the damage zones and from the $l = l_i$ and $D_s = D_s^{(i)}$ results in the undamaged zone.

Second, as a result of specimen preparation and resin curing, the fibre initially has non-zero axial stress. The magnitude of the initial axial stress can vary depending on the amount of fibre prestretching in the mould, the temperature of mixing of resin with hardener and, finally, the curing and post-curing temperatures. When the fibre fractures, there should be a controlled recoil of the fibre. The dynamic fibre recoil depends on the

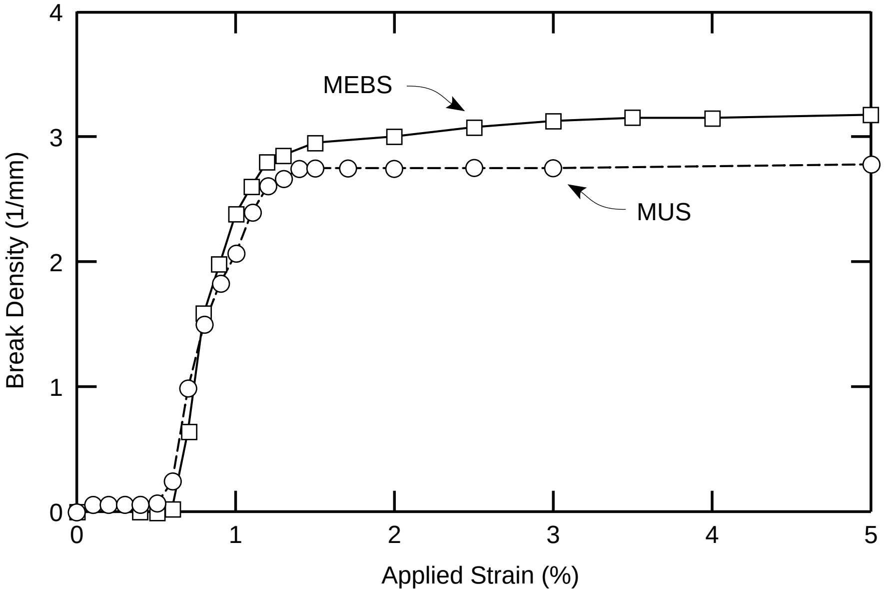

Figure 2. The fibre break density as a function of applied strain during experiments on MEBS/MY750 and MUS/MY750 fragmentation specimens

magnitude of the applied tensile stress, as well as on the residual thermal field and prestretching effects which govern the energy dissipation mechanism and therefore the value of residual axial stress. The amount of recovery of the fibre depends on the strength of the interface. Although the resulting surface of the fibre break should still be stress-free, the spatial resolution of the LRS technique (1 μm) appears to be insufficient for the detection of the point of zero stress at the tip of the fibre. The Bessel-Fourier series solution accounts for residual thermal stresses, but not for prestretching effects. We thus fit experimental results with non-zero stresses at fibre breaks empirically by superposing an additional compressive stress to make the axial fibre stress have the form

$$\langle \sigma_{zz,f} \rangle = \psi_\infty \left(1 - (1 + f_c) \frac{F(z)}{F(l/2)} \right) \tag{8}$$

where f_c the magnitude of the compressive stress observed at fibre breaks as a fraction of the far-field fibre stress (*i.e.*, the stress on the fibre break is $-f_c\psi_\infty$). In fitting experimental results, the value of f_c was chosen to match experimental observations. Finally, as illustrated in Fig. 1, the correction for non-zero fibre-break stress was used only for the stress in the damage zones. The stress in the central, intact zone was calculated using the uncorrected stress in Eq. (1).

RESULTS

Fibre Axial Stress Distributions

MEBS/MY750 (SIZED SYSTEM)

Raman spectra were obtained at large intervals (200 μm) prior to fibre fracture to assess the stress transfer efficiency over the whole length of the embedded fibre. A residual tensile axial stress of about 0.2 GPa was measured at the onset of the experiment, which was attributed to fibre prestretching during specimen preparation. Figure 2 shows the average break density as a function of applied strain. The first fibre breaks appeared at about 0.7% applied strain. The first complete fibre fragments within the selected "window" for Raman measurements were detected at about 1.3% applied strain. Once complete fibre fragments were detected, accurate stress mappings with a resolution of 1 μm on either side of the fibre fracture point were undertaken at intervals of about 0.1% applied strain. Some measured stress profiles over multiple fragments at 1.5%, 2.1%, and 3.05% applied strain are given in Figs. 3–5.

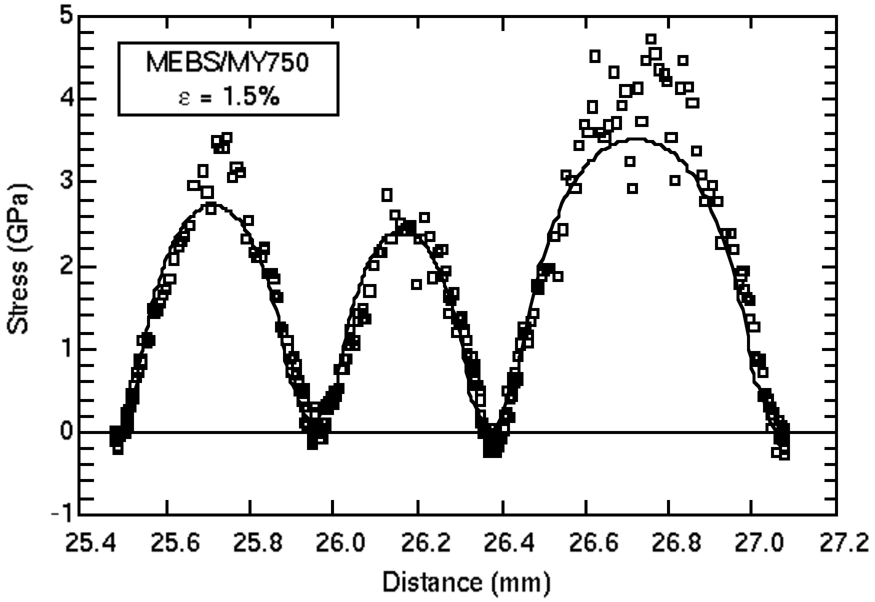

Figure 3. The axial stress in the fibre along several fibre fragments at 1.5% applied strain during a fragmentation test on an MEBS/MY750 specimen. The symbols are experimental points. The smooth curves are fits to the experiments using a two-zone model and the Bessel-Fourier series stress analysis with $D_s^{(i)} = 300$ MPa and $D_s^{(d)}$ and l_d as explained in the text and plotted in Fig. 9.

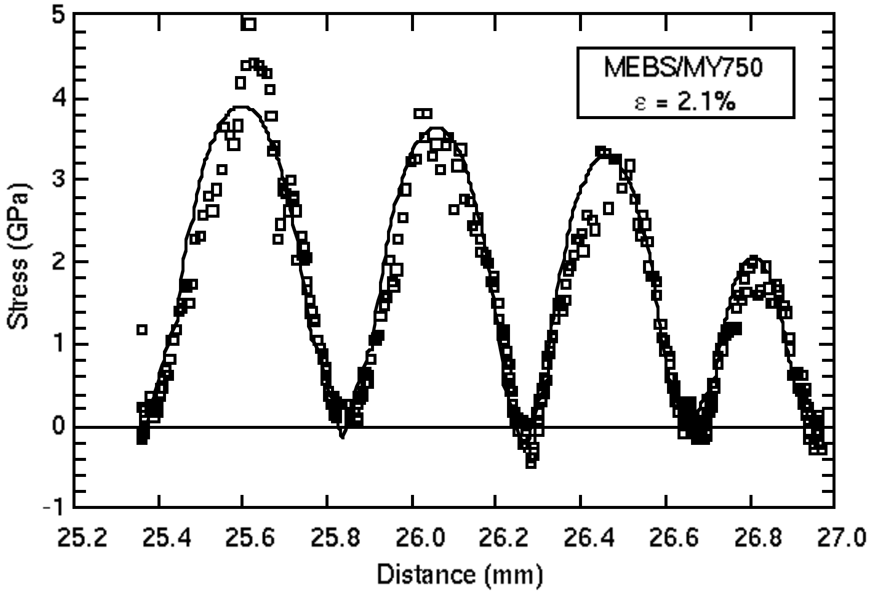

Figure 4. The axial stress in the fibre along several fibre fragments at 2.1% applied strain during a fragmentation test on an MEBS/MY750 specimen. The symbols are experimental points. The smooth curves are fits to the experiments using a two-zone model and the Bessel-Fourier series stress analysis with $D_s^{(i)} = 300$ MPa and $D_s^{(d)}$ and l_d as explained in the text and plotted in Fig. 9.

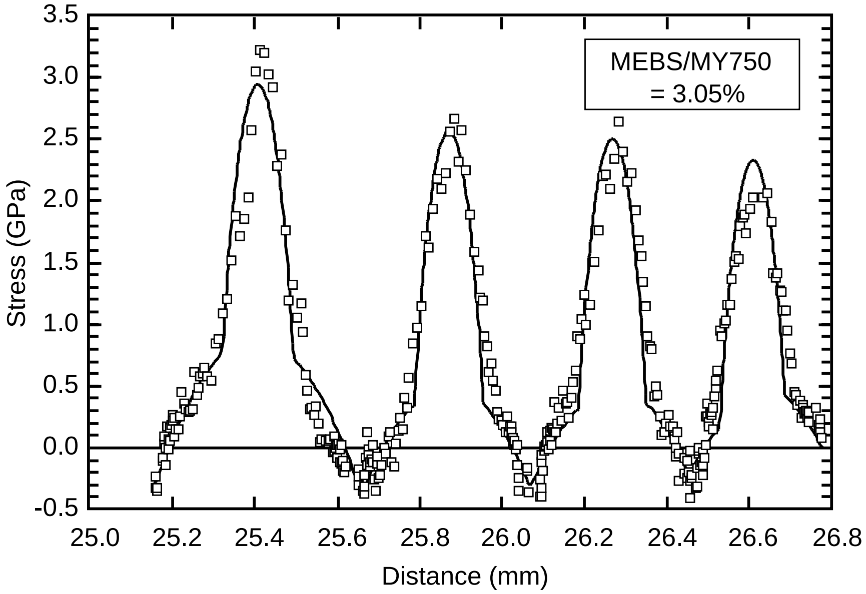

Figure 5. The axial stress in the fibre along several fibre fragments at 3.05% applied strain during a fragmentation test on an MEBS/MY750 specimen. The symbols are experimental points. The smooth curves are fits to the experiments using a two-zone model and the Bessel-Fourier series stress analysis with $D_s^{(i)} = 300$ MPa and $D_s^{(d)}$ and l_d as explained in the text and plotted in Fig. 9.

At an applied strain of 1.5%, four distinct fibre fractures and three complete fibre fragments were observed in the Raman “window” (see Fig. 3). There was only a small amount of compressive stress at the fibre breaks and there was a hint of interfacial damage zones near fibre breaks. The damage zones are indicated by a slight change in the rate of stress transfer at distances of about 30 to 40 μm from the fibre breaks (or 6 to 7 fibre diameters). At an applied strain of 2.1% (see Fig. 4) there was an additional fibre break and therefore an additional fibre fragment. Both the compressive axial stress at the fracture point and the size of the damage zones increased as the applied strain increased from 1.5% to 2.1%. These results indicate some form of interfacial failure [4] had propagated further as the applied strain increased. By 3.05% (see Fig. 5) applied strain, the damage zones became very pronounced and extended distances of about 100 μm from each fibre break. The damage zones became even more apparent at applied strains higher than 3.05%.

MUS/MY750 (UNSIZED SYSTEM)

As done with the MEBS sized system, Raman spectra for the MUS unsized system were obtained at large intervals (200 μm) prior to fibre fracture to assess the integrity and stress transfer efficiency of the whole coupon. A residual compressive axial stress of about −0.3 GPa was measured at the onset of the experiment. This stress was attributed to thermal shrinkage of the resin during curing, which was not offset by fibre prestretching during specimen preparation (as was the case for the MEBS system). Figure 2 shows the average break density as a function of applied strain. The first fibre breaks appeared at about 0.6% applied strain. The saturation break density was lower (or the critical fragment length was longer) for the MUS system then for the MEBS system. The first complete fibre fragments within the selected “window” for Raman measurements were detected at about 1.2% applied strain. Once complete fibre fragments were detected, accurate stress mappings with a resolution of 1 μm on either side of the fibre fracture point were undertaken at intervals of about 0.1% applied strain. Some measured stress profiles over multiple fragments at 1.6%, 2.1%, and 2.65% applied strain are given in Figs. 6–8.

At an applied strain of 1.6%, six distinct fibre fractures and five complete fibre fragments were observed in the Raman “window” (see Fig. 6). The residual compressive stress at the fibre breaks was larger for MUS specimens than at the corresponding strain with MEBS specimens. This larger compressive stress may have been caused by the differing initial axial stresses prior to the experiment. At 1.6% applied strain there were indications a interfacial damage zones near fibre breaks of about 40 μm (7 or 8 fibre diameters).

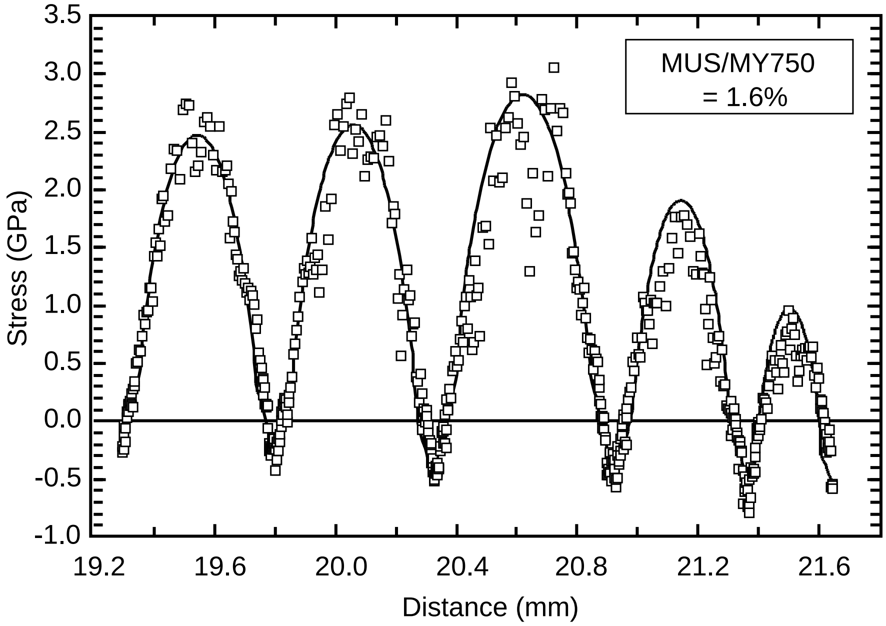

Figure 6. The axial stress in the fibre along several fibre fragments at 1.6% applied strain during a fragmentation test on an MUS/MY750 specimen. The symbols are experimental points. The smooth curves are fits to the experiments using a two-zone model and the Bessel-Fourier series stress analysis with $D_s^{(i)} = 150$ MPa and $D_s^{(d)}$ and l_d as explained in the text and plotted in Fig. 9.

At an applied strain of 2.1% (see Fig. 7) there were an identical number of fibre breaks and fragments in the same Raman "window". As with the MEBS system, however, all damage zones increased in size as the applied strain increased from 1.6% to 2.1%. Finally, at 2.65% applied strain, the damage zones became very pronounced and extended distances of about 90 μm from each fibre break.

Two-Zone Bessel-Fourier Data Analysis

All experimental Raman results were analyzed by fitting to the two-zone model in Fig. 1B. For both MEBS and MUS, we sought fits for which stress transfer in the central, intact zone was independent of the damage that had occurred near the fibre breaks. In other words, $D_s^{(i)}$ was taken as a strain-independent material property of the interphases in each specimen type. Furthermore f_c was set to zero for the central, intact zones. The intact zones of all MEBS specimens could be fit using $D_s^{(i)} = 300$ MPa; the intact zones of all MUS specimens could be fit using $D_s^{(i)} = 150$ MPa. We emphasize that although $D_s^{(i)}$ was assumed to be constant in the fitting process, the fact the we could fit all results successfully means that a constant $D_s^{(i)}$ is an experimental finding. In other words, we could not resolve changes in $D_s^{(i)}$ for a single fibre type by allowing it to be a strain-dependent quantity. The differences between the $D_s^{(i)}$ values for these two fibres are significant in that we have resolved differences in stress transfer properties; the results show that stress transfer is more efficient in the sized MEBS specimen than in the unsized MUS specimens. The factor of two difference, however, may overstate the differences. The change in stress transfer rate is not linearly related to $D_s^{(i)}$. Some example plots in Ref. [9] show the effect of $D_s^{(i)}$ on stress transfer rate over the range of $D_s^{(i)}$ from 0 to ∞. the difference between a $D_s^{(i)} = 300$ MPa and a $D_s^{(i)} = 150$ MPa are resolvable, but not dramatic.

When including the damage zones in the analyses, there were three factors to consider. First, we needed to select the length of the damage zone, l_d. It is difficult to determine l_d directly from Raman data or by microscopy observations using photoelasticity. We argue, however, that our fitting process made the selection of l_d less ambiguous. If l_d was chosen incorrectly, the fits in the central, intact zone would suffer; by monitoring the entire fitting process we were thus able to narrow in on the correct l_d or at least a value of l_d that is consistent with all other experimental observations. Second, there was often some asymmetry

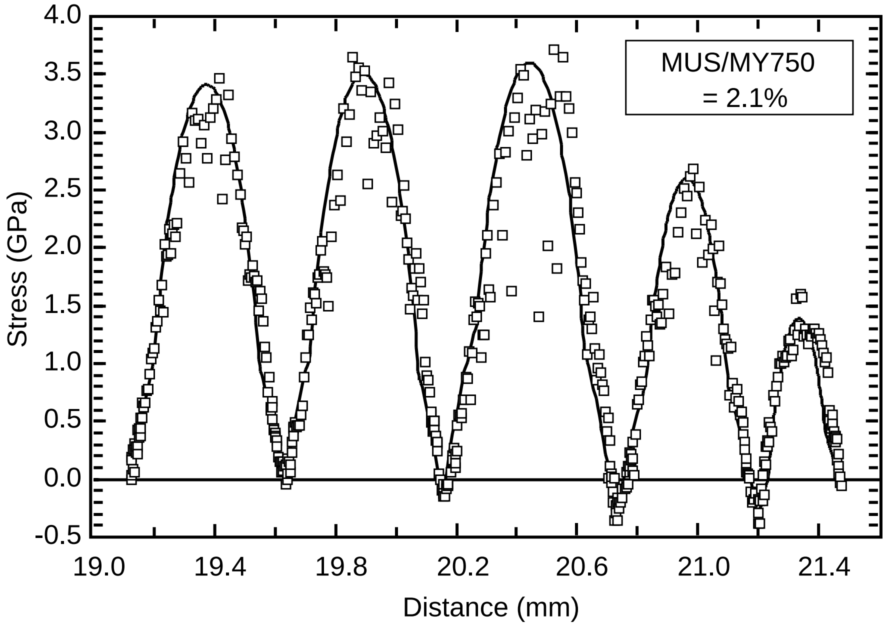

Figure 7. The axial stress in the fibre along several fibre fragments at 2.1% applied strain during a fragmentation test on an MUS/MY750 specimen. The symbols are experimental points. The smooth curves are fits to the experiments using a two-zone model and the Bessel-Fourier series stress analysis with $D_s^{(i)} = 150$ MPa and $D_s^{(d)}$ and l_d as explained in the text and plotted in Fig. 9.

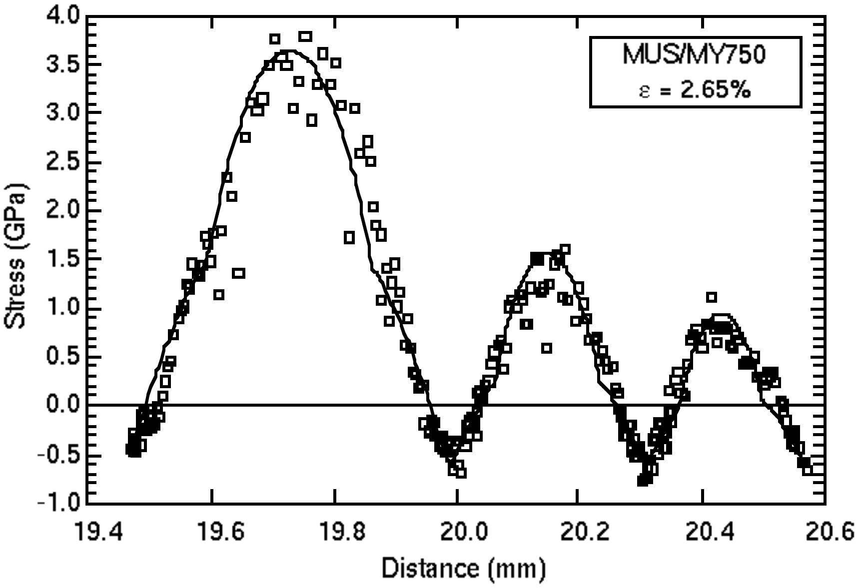

Figure 8. The axial stress in the fibre along several fibre fragments at 2.65% applied strain during a fragmentation test on an MUS/MY750 specimen. The symbols are experimental points. The smooth curves are fits to the experiments using a two-zone model and the Bessel-Fourier series stress analysis with $D_s^{(i)} = 150$ MPa and $D_s^{(d)}$ and l_d as explained in the text and plotted in Fig. 9.

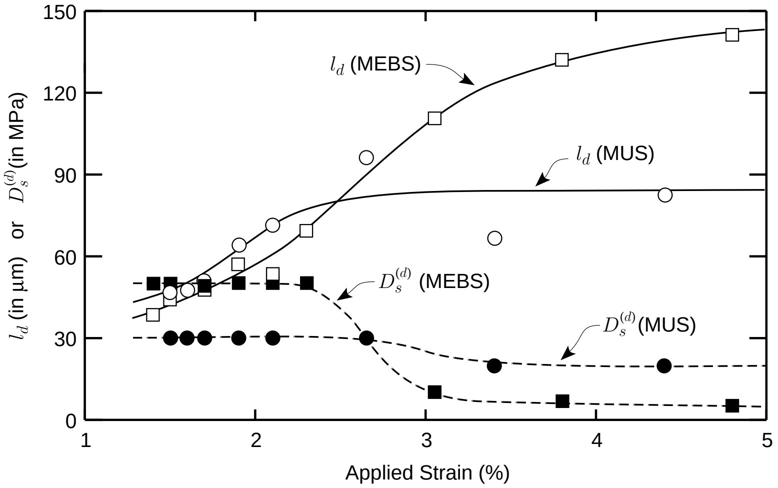

Figure 9. The average damage zone length, l_d (in μm), and the imperfect interface parameter in the damage zone, $D_s^{(d)}$ (in MPa), as function of applied strain for both MEBS and MUS fragmentation specimens.

within a single fragment where the damage zone on one side of a fragment was different in length than the damage zone on the other side. To account for this asymmetry, each fragment was split in half and the two halves were fit independently. Then, the two halves were pieced together to give a fit for the full fragment. Third, the rate of stress transfer in the damage zones could not be fit with a single value of $D_s^{(d)}$. The stress transfer in the damage zones was clearly slower at high strain than at low strain. Mathematically, this effect corresponds to $D_s^{(d)}$ being a strain-dependent quantity. Physically, a decrease in $D_s^{(d)}$ at high strain corresponds to an increase in interfacial damage within the damage zones which leads to increased impairment of stress transfer. Note that if $D_s^{(d)}$ is viewed purely as a mathematical means of reducing a three-dimensional interphase zone to two-dimensional interface then $D_s^{(d)}$ should be independent of strain. We thus take the strain-dependence to indicate development of damage. One possibility is non-linearity or plastic yielding in the matrix local to the interface. Even if there is yielding, however, our linear-elastic analysis with a strain-dependent $D_s^{(d)}$ can still be viewed as a viable analysis method. In effect, we are lumping local yielding effects into the interface parameter. The situation is analogous to linear-elastic fracture mechanics with small-scale yielding where an effective crack length in a linear-elastic analysis can be used to correct for crack-tip yield zones [18].

To analyze Raman experiments at each level of applied strain, we used the $D_s^{(i)}$ appropriate for the material being analyzed, selected an optimal $D_s^{(d)}$ for that strain level, and adjusted the damage zone lengths, l_d, of each damage zone until a good fit was obtained. We were able to obtain good fits for all fragments at all applied strains. Typical fit results for selected strain levels are shown in Figs. 3–8. From the fit results we can calculate the average damage zone size and $D_s^{(d)}$ within the damage zones as a function of applied strain. Those results are plotted in Fig. 9. At low strain the damage zone sizes in MEBS and MUS were similar, but slightly higher in MUS. At high strain, the damage zones in MEBS saturated at about 140 μm while the damage zones in MUS saturated at about 90 ± 10 μm. At low strain $D_s^{(d)}$ in MEBS was about 50 MPa which is greater than the $D_s^{(d)} = 30$ MPA in MUS. At high strain, the situation reverses with $D_s^{(d)}$ in MUS dropping to about 20 MPa which is greater than the high-strain $D_s^{(d)} = 5$ MPa in the MEBS specimen. We can also calculate the end-stress correction factor, f_c, required to fit the non-zero fibre break stress in the damage zones. The results were scattered, but roughly independent of applied strain. In MEBS, $f_c = 0.2 \pm 0.1$ while in MUS, $f_c = 0.4 \pm 0.2$. The larger value in MUS was probably caused by the more compressive initial axial stress prior to starting the fragmentation experiments.

DISCUSSION

By fitting LRS results for average axial stress in the fibre as a function of position from fibre breaks to the Bessel-Fourier series stress analysis, we were able to measure stress transfer properties of an intact interface, $D_s^{(i)}$, stress transfer properties of a damaged interface, $D_s^{(d)}$, and the size of the damage zones, l_d. For the intact zones, $D_s^{(i)} = 300$ MPa for the MEBS fibres and $D_s^{(i)} = 150$ MPa for the MUS fibres. For each fibre type, a single-value of $D_s^{(i)}$ sufficed for fitting results at all applied strain levels. Thus we claim that $D_s^{(i)}$ is a useful material property characterizing the interfaces in these specimens. The factor of two difference is a significant difference. In other words, the fitting procedure allowed us to clearly distinguish between MEBS and MUS fibres. The stress transfer efficiency for the sized or MEBS fibres was better than for the unsized or MUS fibres.

LRS experiments on fibres embedded in real laminates or in multi-fibre specimens [15] show some differences from the LRS experiments described here on single embedded fibres. Because laminates cannot be strained to the high strain levels used for single-fibre specimens, the damage zones near fibre-breaks in laminates are much smaller. Furthermore, fibre breaks in laminates do not show the recoil-induced, compression stresses at fibre breaks [15]. Because the intact zone thus dominates in *real* laminates, we claim that the role of the interface in *real* laminates is determined much more by $D_s^{(i)}$ than by the damage zone properties $D_s^{(d)}$ and l_d. Furthermore, if $D_s^{(i)}$ is a mechanical property of the interface or interphase zone, then it might be expected to be the same in both single-fibre specimens and in real laminates. If true, then the potential exists to direct translation of results on single-fibre specimens to predictions about properties of real laminates. This potential can be examined by measuring laminate properties and comparing those predictions to effective property theories that include an imperfect interface [12].

In the absence of LRS results, fragmentation experiments are often interpreted in terms of an interfacial shear strength, τ_{ISS}, calculated by

$$\tau_{ISS} = \frac{r_f \sigma_f(l_c)}{l_c} \tag{9}$$

where l_c is the *critical* fragment length and $\sigma_f(l_c)$ is the strength of the fibre with a length of l_c. The critical length is given by

$$l_c = f\langle l \rangle \tag{10}$$

where $\langle l \rangle$ is the average fragment length when the fragmentation process ceases and f is a factor introduced to account for distributions in final fragment length; it is commonly assumed to be 4/3 [19]. We argue that the critical length, however it is calculated, is strongly influenced by the damage zone properties $D_s^{(d)}$ and l_d [11]. Because $D_s^{(d)}$ and l_d are unimportant for determining the role of the interface in real laminates, τ_{ISS} will similarly give little information about that role. The preferred interfacial property to measure is $D_s^{(i)}$.

Although $D_s^{(d)}$ and l_d are less important than $D_s^{(i)}$, they still give information about interfacial failure properties. At low strain, the damage zone sizes for MUS fibres are slightly larger than for MEBS fibres and the value of $D_s^{(d)}$ is slightly lower for MUS fibres than for MEBS fibres. These results both suggest that the interface for MUS fibres is weaker than for MEBS fibres. At higher strain, however, the situation reverses — the damage zones are smaller and $D_s^{(d)}$ is higher for the MUS fibres *vs.* the MEBS fibres. These seemingly contradictory results can be explained by energy calculations and the effect of $D_s^{(i)}$ on the energy released when the fibre fragments [11]. When $D_s^{(i)}$ is lower, the amount of energy released by the first few fibre breaks is higher than when $D_s^{(i)}$ is higher [11]. Physically, when $D_s^{(i)}$ is lower, the extra interfacial slip allows more energy to be released. Thus, the results at low strain may be a consequence of $D_s^{(i)}$ being lower for MUS fibres than for MEBS fibres. Like the experimental results, the energy calculations reverse at high strain. When $D_s^{(i)}$ is lower, the amount of energy released during high strain breaks is lower than when $D_s^{(i)}$ is higher [11]. Physically, the energy was already released at low strain and therefore not available at high strain. Thus, the extra damage growth with MEBS fibres may be a consequence of $D_s^{(i)}$ being higher for MEBS than for MUS fibres. In summary, it is difficult to compare damage zone measurements for two fibres that have different values of $D_s^{(i)}$. Curiously, among a group of fibres with similar interfacial toughness properties, the fibres with the better interfaces, as judged by the value of $D_s^{(i)}$, will actually have the *most*

Table 2. The interfacial shear strength (τ_{ISS} in MPa) calculated from the critical fragment length or from the maximum shear stress measured in LRS experiments.

Fibre Type	From Critical Length	From Raman
MEBS	30.1 ± 0.9	41.9 ± 7.2
MUS	25.9 ± 0.9	36.8 ± 6.5

damage at saturation. Failure to account for this effect and interpretation of results based on the amount of damage around critical-length fragments may lead to invalid conclusions about interfacial properties.

The interfacial shear strength, τ_{ISS}, can be estimated from the critical length (using Eqs. (9) and (10) with $f = 4/3$). Interfacial shear stress can also be directly measured by differentiating the LRS results for axial fibre stress [5]; the peak of this measured shear stress is a direct measurement of τ_{ISS}. The results of these two approaches to finding τ_{ISS} are given in Table 2. Both methods predict that the MEBS interface is better than the MUS interface. The LRS results, which measures the peak shear stress, gives a higher result than the critical length method, which determines an average shear stress. The differences in τ_{ISS} between MEBS and MUS are much smaller than the differences recorded when measuring $D_s^{(i)}$. Besides peak shear stress, the LRS experiments can provide axial and interfacial shear stress distributions at each level of applied strain, measure transfer lengths, and determine zones of interfacial damage. The peak of the interfacial shear stress distribution measured by LRS is obviously affected by the presence of interfacial damage. As reported earlier [4], the MEBS interface exhibits higher values of maximum interfacial shear stresses (peak of ISS distribution), which are responsible for inducing more prominent interfacial damage at high applied strains. This extra damage, in turn, leads to a subsequent decrease in the maximum value of ISS as a function of applied strain [4], and is masking the real differences in the stress transfer efficiency between the two systems. Hence, an effective characterization of the interface requires separation of the intact and damaged zones as attempted here. In terms of interface parameters, τ_{ISS} is influenced by $D_s^{(i)}$ with higher values of $D_s^{(i)}$ tending to reduce τ_{ISS}. Thus the higher value of $D_s^{(i)}$ for MEBS fibres probably reduced its τ_{ISS} and therefore masked the difference between the two fibre types. Finally, the extensive interfacial damage that takes place during the fragmentation test at relatively high strains is hardly, if at all, present at low *service* strains. Recent LRS experiments on short fibre model coupons at low strains ($< 0.6\%$) where interfacial damage is negligible and elastic behaviour can be assumed, indicate that the MEBS interface is stronger than that of MUS by a factor of 2 [20]. This result is in perfect agreement with the $D_s^{(i)}$ values calculated by the Bessel-Fourier analysis of the two systems. The conclusion is that the $D_s^{(i)}$'s obtained here by the combined LRS/Bessel-Fourier series analysis fully characterizes the efficiency of the interface and can have a universal validity for other composite systems as well.

CONCLUSIONS

By analyzing simultaneous fragmentation and LRS experiments it is possible to get much information about fibre-matrix interfacial properties. By fitting measured axial fibre stress to the Bessel-Fourier series stress analysis in undamaged regions of the fibre/matrix interface, it is possible to measure an interfacial stress transfer property denoted here as $D_s^{(i)}$. We claim $D_s^{(i)}$ is best property for predicting the role of the interface in real composite laminates. The higher the value of $D_s^{(i)}$, the better the interface where better here means more efficient stress transfer. Furthermore, the higher $D_s^{(i)}$, the smaller the amount of energy released when a fibre breaks at low strain (*i.e.*, the strains typically experienced in real laminates) and thus the less interfacial damage that will be caused by those breaks.

Fragmentation tests are typically continued to high strain or until the fragmentation process ceases. By analyzing LRS experiments as a function of strain it is possible to follow the length of the interfacial damage zone (l_d) and the extent of interfacial damage (characterized by the value of $D_s^{(d)}$). From LRS results and from critical fragment length results it is also possible to deduce an interfacial shear strength (τ_{ISS}). We claim that these high-strain observations from fragmentation tests are less useful for characterizing the fibre/matrix interface. Furthermore, these damage properties are all influenced by the value of $D_s^{(i)}$. A "good" interface, that is one with high $D_s^{(i)}$, leads to the presence of more damage at high strains than that observed in a system with a "poor" interface. The presence of such damage can mask the difference between the two systems. In this work, the Bessel-Fourier analysis indicates that the sized system exhibits better stress-transfer efficiency than the the unsized system. The presence of interfacial damage, however, drastically reduces this difference, and the sized system exhibits a meagre 14-16% stronger interface as measured by interfacial shear stress (see Table II). Thus the fragmentation test data can only be unambiguously interpreted if the interfacial damage zone is fully identified and distinguished from the intact interface (low strain data). This approach is important because the intact interface properties, described through the single parameter $D_s^{(i)}$, are more likely to dominate the behavior of real composites. Finally, we claim that combining LRS experiments with Bessel-Fourier series stress analysis is a viable method for determining the $D_s^{(i)}$ interface property.

ACKNOWLEDGEMENTS

The authors would like to thank CEC for financial support under the Brite-Euram CT-91-9503 project, Soficar (Toray) Industries, France for providing the fibres. The QMW team would also like to thank the EPSRC and AGARD for support given to the Raman Group. The UU team was supported, in part, by a grant from the Mechanics of Materials program at NSF (CMS-9401772), and , in part, by a grant from the United States-Israel Binational Science Foundation (BSF Grant No. 92-00170), Jerusalem, Israel

REFERENCES

1. Drzal, L. T., M. J. Rich, and P. F. Lloyd 1983. "Adhesion of Graphite Fibers to Epoxy Matrices: I. The Role of Fiber Surface Treatment," *J. Adhesion*, 16:1–30.
2. Kelly, A. and W. R. Tyson 1965. "Tensile Properties of Fibre-Reinforced Metals: Copper/Tungsten and Copper/Molybdenum," *J. Mech. Phys. Solids*, 13:329–350.
3. Lacroix, Th., B. Tilmans, R. Keunings, M. Desaeger, and I. Verpoest 1992. "Modeling of Critical Fibre Length and Interfacial Debonding in the Fragmentation Testing of Polymer Composites," *Comp. Sci. & Tech.*, 43:379–387.
4. Paipetis, A. and C. Galiotis 1996. "Effect of Fibre Sizing on the Stress Transfer Efficiency in Carbon/Epoxy Model Composites," *Composites Part A*, 27A:755–767.
5. Melanitis, N., C. Galiotis, P. L. Tetlow, and C. K. L. Davies 1992. "Interfacial Shear Stress Distribution in Model Composites Part 2: Fragmentation Studies on Carbon Fibre/Epoxy Systems," *J. Comp. Mat.*, 26:574–610.
6. Melanitis, N., C. Galiotis, P. L. Tetlow, and C. K. L. Davies 1993. "Interfacial Shear Stress Distribution in Model Composites: The Effect of Fiber Modulus," *Composites*, 24:459–466.
7. Melanitis, N., C. Galiotis, P. L. Tetlow, and C. K. L. Davies 1993. "Monitoring the Micromechanics of Reinforcement in Carbon Fibre/Epoxy Resin Systems," *J. Mat. Sci.*, 28:1648–1654.
8. Nairn, J. A. 1997. "On the Use of Shear-Lag Methods for Analysis of Stress Transfer in Unidirectional Composites," *Mech. of Materials*, 26:63–80.
9. Nairn, J. A. and Y. C. Liu 1997. "Stress Transfer into a Fragmented, Anisotropic Fiber Through and Imperfect Interface," *Int. J. Solids Structures*, 34:1255–1281.
10. Nairn, J. A., Y. Ching Liu, and C. Galiotis 1995. "Analysis of Stress Transfer from the Matrix to the Fiber Through an Imperfect Interface: Application to Raman Data and the Single-Fiber Fragmentation Test," *ASTM STP 1290*, pp. 47–65.
11. Nairn, J. A. and Y. C. Liu 1997. "On the Use of Energy Methods for Interpretation of Results of Single-Fiber Fragmentation Experiments," *Composite Interfaces*, 4:241–267.
12. Hashin, Z. 1990. "Thermoelastic Properties of Fiber Composites With Imperfect Interface," *Mech. of Materials*, 8:333–348.
13. Galiotis, C. and D. N. Batchelder 1988. "Strain Dependence of the First- and Second-Order Raman Spectra of Carbon Fibres," *J. Mater. Sci. Letts.*, 7:545–547.
14. Galiotis, C. 1993. "A Study of Mechanisms of Stress-Transfer in Continuous and Discontinuous Fibre Model Composites Using Laser Raman Spectroscopy," *Comp. Sci. & Tech.*, 48:15–28.
15. Galiotis, C., V. Chohan, A. Paipetis, and C. Vlattas 1995. "Interfacial Measurements in Single and Multi-Fiber Composites Using the Technique of Laser Raman Spectroscopy," *ASTM STP 1290*, pp. 19–33.

16. Paipetis, A., C. Vlattas, and C. Galiotis 1996. "Remote Laser Raman Microscopy (ReRaM); Part 1: Design and Testing of a Confocal Microprobe," *J. Raman. Spect.*, 27:519–526.
17. Arfken, G. 1970. *Mathematical Methods for Physicists*. New York, Academic Press.
18. Williams, J. G. 1984. *Fracture Mechanics of Polymers*, New York, John Wiley & Sons.
19. DiLandro, L. and M. Pegorano 1987. "Carbon Fibre-Thermoplastic Matrix Adhesion," *J. Mat. Sci.*, 22:1980–1986.
20. Galiotis, C. and A. Paipetis 1998. "Definition and Measurement of the Shear-Lag Parameter β as an Index of the Stress Transfer Efficiency of Polymer Composites," *J. Mat. Sci.*, 33:1137–1143.